AGU
ADVANCING EARTH AND SPACE SCIENCES

Geophysical Research Letters®

Key Points:

- About 80% of the sea level changes over the South China Sea (SCS) shelves are attributed to the redistribution of ocean mass from deeper regions
- The SCS throughflow has exhibited a weakening trend over the past six decades
- Steric sea level changes, driven by fluctuations in Luzon Strait transport, dominate long-term sea level variations in the SCS

Supporting Information:

Supporting Information may be found in the online version of this article.

Correspondence to:

B. Thompson,
bijoymet@gmail.com

Author Contributions:

Conceptualization: B. Thompson
Formal analysis: B. Thompson, S. Jevrejeva, J. Zachariah, D. G. Faller, P. Tkalich
Funding acquisition: B. Thompson
Investigation: B. Thompson
Methodology: B. Thompson, S. Jevrejeva, J. Zachariah, D. G. Faller, P. Tkalich
Project Administration: P. Tkalich
Software: B. Thompson, J. Zachariah, D. G. Faller
Supervision: B. Thompson, P. Tkalich
Writing – original draft: B. Thompson

Impact of Mass Redistribution on Regional Sea Level Changes Over the South China Sea Shelves

B. Thompson[1,2] , **S. Jevrejeva[3]** , **J. Zachariah[1], D. G. Faller[1], and P. Tkalich[1,2]**

[1]Tropical Marine Science Institute, National University of Singapore, Singapore, Singapore, [2]Technology Center for Offshore and Marine Singapore, Singapore, Singapore, [3]National Oceanography Centre, Southampton, UK

Abstract This study investigates long-term sea level changes in the South China Sea (SCS) using a validated high-resolution regional ocean model simulation for the Maritime Continent. The contributions of ocean mass redistribution and steric sea level are examined to understand the sea level variations. The ocean bottom pressure (OBP) serves as an indicator of sea level variations linked to alterations in ocean mass flux. The OBP accounts for over 80% of the total sea level change over the shelves, while the steric sea level emerges as the dominant factor, contributing over 50% to the sea level change in the deep SCS. Luzon Strait transport shows a weakening trend in the last six decades, resulting in higher heat accumulation and larger steric expansion in the deep SCS. The ocean mass redistribution acts as a mechanism to balance the contrasting steric induced sea level changes over the deep SCS and shallow continental shelves.

Plain Language Summary The South China Sea (SCS) has vast continental shelves covering more than half of its surface area. The study investigates long-term sea level changes in the SCS using an ocean general circulation model simulation, considering steric sea level (water expansion due to temperature and salinity changes) and ocean mass redistribution. The analysis showed a significant increase in steric sea level in the deep SCS, while the contribution of ocean mass redistribution decreased. The mass redistribution was responsible for over 80% of the total sea level change, except in the deep SCS, where steric sea level dominated. Weakened flow from the Pacific Ocean to the SCS led to more heat accumulation and higher steric expansion in the deep SCS, causing water to redistribute toward the shelves.

1. Introduction

According to the Intergovernmental Panel on Climate Change Assessment Report 6 (IPCC AR6 Synthesis Report, 2023), the Global Mean Sea Level (GMSL) increased by about 0.20 m between 1901 and 2018. The GMSL is *likely* to rise between 0.28 and 0.55 m relative to 1995–2014 under the lowest greenhouse gas emission scenario SSP1-1.9, and between 0.63 and 1.01 m under the very high emission scenario SSP5-8.5 by the year 2100. The sea level rise (SLR) is characterized by substantial deviations from the global mean across various regions of the world ocean (e.g., Fox- Kemper et al., 2021). The regional SLR behavior can be attributed to (a) steric sea level changes arising from thermo-halosteric expansion and ocean mass redistribution through ocean circulation (Chen et al., 2021; Gregory et al., 2019), (b) gravitational, rotational, and deformational (GRD) effects resulting from land ice discharge and groundwater storage (Mitrovica et al., 2001), and (c) vertical and horizontal land movements driven by glacial isostatic adjustment (Peltier, 2004). The combined effects of steric and mass redistribution on sea level changes are commonly referred to as sterodynamic sea level (Gregory et al., 2019).

The South China Sea (SCS) is recognized as one of the largest marginal seas in the West Pacific Ocean, characterized by its complex geometry attributed to the presence of continental shelves, islands and numerous straits. It is distinguished by deep oceanic regions with depths exceeding 3,000 m in the central area, while the southern and northwestern regions are characterized by continental shelves having depth less than 200 m (Figure 1). In our study, we define shelves as the oceanic regions where the depth does not exceed 200 m (e.g., Amiruddin et al., 2015). In addition, we designate the shelf region between 2°S and 14°N within the SCS as the Sunda Shelf, and the shelf area north of 14°N in the western SCS as the northwestern shelf. The steric sea level changes occur primarily through the warming or cooling of the ocean and it cannot fully explain the sea level changes over the shallow sea shelves (Landerer et al., 2007). By employing a simple mass redistribution model, Landerer et al. (2007) suggested a net mass transfer from deep oceanic regions to the shallow shelf seas as a plausible mechanism to account for the SLR over the sea shelves. The monitoring of ocean bottom pressure (OBP)

Writing – review & editing: S. Jevrejeva, P. Tkalich

demonstrates to be an effective method in comprehending the contribution of mass redistribution to sea level changes, as the alterations in sea level attributed to ocean circulation are closely linked to changes in ocean mass (Chen et al., 2021; Landerer et al., 2007).

Studies investigating the relative contributions of steric and mass redistribution to the long-term sea level changes observed in the SCS are very limited. Previous studies have predominantly relied on relatively coarse-resolution global climate models, coarse-resolution grided observational data, or satellite observations covering relatively short time periods (e.g., Cheng & Qi, 2010; Qu et al., 2019). Understanding the drivers of sea level changes over the sea shelves is essential for coastal vulnerability assessment and the development of adaptation strategies. The present study aims to investigate the physical mechanisms responsible for the sea level changes in the SCS shelves, with a particular emphasis on the ocean mass redistribution processes. To accomplish this, we utilize hindcast simulations from a high-resolution regional ocean model, configured for the Maritime Continent (MC), covering the period from 1961 to 2022.

2. Model and Data

A regional version of Océan Parallélisé ocean engine within the Nucleus for European Modeling of the Ocean (NEMO v4.0.6) (Madec et al., 2016) framework configured for the MC domain 90°–142°E, 18°S–27°N is employed in the study (Figure 1). NEMO is a primitive-equation, hydrostatic, Boussinesq ocean model extensively used in climate modeling studies (e.g., Zuo et al., 2019). The Boussinesq approximation employed in the NEMO model conserves volume rather than mass and hence does not model all the components of steric expansion prognostically. Therefore, the model employed in the current study includes the local steric effect while not incorporating the global mean and non-Boussinesq steric effects.

The model has a horizontal resolution of 4.5 km × 4.5 km and 51 vertical levels in terrain-following coordinate system. The model has been integrated from January 1959 to October 2022, forced by the European Centre for Medium Range Weather Forecasting (ECMWF) Reanalysis 5 (ERA5) (Hersbach et al., 2020) at the surface boundaries, and ECMWF Ocean Reanalysis System 5 (ORAS5) (Zuo et al., 2019) at the lateral ocean boundaries. The model hindcast simulations during January 1961 to October 2022 is used for further analysis in the study.

The estimation of steric sea level change is performed using the model-simulated temperature and salinity fields (details in the supplementary information). The OBP serves as an indicator of sea level variations linked to alterations in ocean mass flux. The OBP variations due to atmospheric pressure, known as the inverse barometer effect, are removed from the model simulations before analysis since their influence on ocean dynamics is negligible in timescales beyond a few days (Wunsch & Stammer, 1997). In our study, we utilize the equivalent water depth of OBP to represent the contribution of sea level change due to ocean mass redistribution.

For the validation of model Sea Surface Height (SSH) simulation, the monthly averaged tide gauge records from 24 locations (Figure 1) within the SCS are obtained from the Permanent Services for Mean Sea Level (Holgate et al., 2013) and merged satellite SSH observation product from Copernicus Marine Environment Monitoring Service (https://doi.org/10.48670/moi-00145) are employed in the study.

3. Results and Discussion

3.1. Model Sea Surface Height

The comparison of the time mean SSH from the model and Mean Dynamic Topography (MDT) from satellite observations is presented in Figures 2a and 2b, respectively. Both, the model and satellite data exhibit an identical spatial pattern, with higher mean SSH in the northwestern tropical Pacific Ocean and lower values in the northwestern equatorial Pacific Ocean, as well as in the eastern tropical Indian Ocean south of the Sumatra and Java Islands. Within the SCS, positive MDT anomalies are observed south of 15°N, with peak values in the Gulf of Thailand. The wind forcing is known to be the dominant factor driving sea level variations in these regions (Amiruddin et al., 2015).

Furthermore, a comparison is made between the monthly averaged sea surface height anomaly (SSHA) derived from the model, tide gauge measurements and satellite observations (Figures S1–S6 in Supporting Information S1). Given the potential unavailability of SSH data from the model and satellite observations at the exact tide gauge location, the data from the nearest grid point is considered instead. To ensure an accurate representation and to assess the model's sea level simulation within the SCS, tide gauge stations were selected in locations including the Malacca Strait, Singapore Strait, eastern coast of the Malay Peninsula, west coast of Borneo Island,
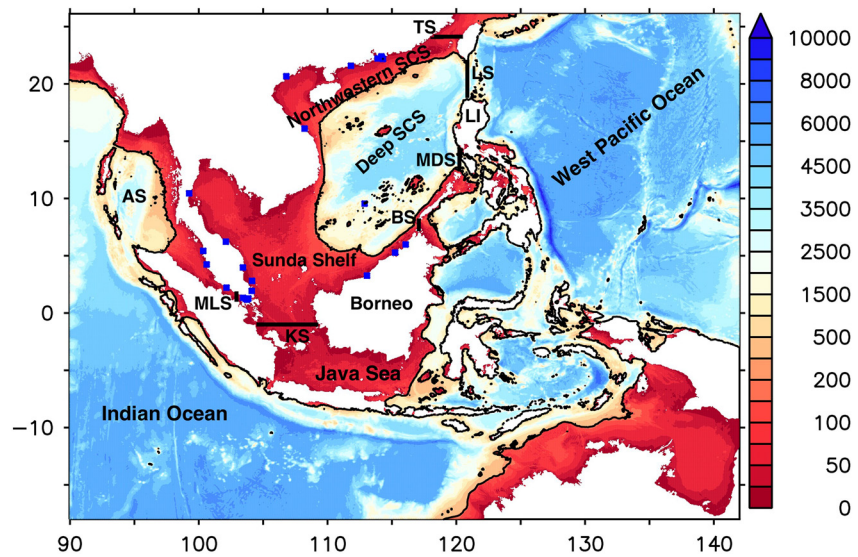
Figure 1. Model Domain and bathymetry in meters (GEBCO Compilation Group, 2020) with the 200 m contour lines. The sections used for volume transport computation across various straits are shown as thick lines. The locations of tide gauges used in the analysis are shown as blue boxes. LS, Luzon Strait; LI, Luzon Island; TS, Taiwan Strait; MDS, Mindoro Strait; BS, Balabac Strait; KS, Karimata Strait; MLS, Malacca Strait; AS, Andaman Sea.

Gulf of Thailand, Gulf of Tonkin and the Hong Kong region (Figure 1). Correlation analysis between the satellite and model as well as the tide gauge records and model, yields statistically significant correlations above the 99.9% confidence level. The comparison of SSHA derived from the model, against tide gauge and satellite measurements illustrate that the sea level changes over the SCS region is reproduced well by the model, and thereby confirming the model's accuracy in capturing the observed SSHA patterns.

In this study, we acknowledge limitations in comparing tide-gauge and satellite sea level observations. Satellite observations may lack accuracy when compared with tide gauges, which are positioned along the coast. Additionally, tide gauge observations can be influenced by local land movements. It is worth to note that satellite and tide gauge observations were exclusively employed for model validation in the present study. Moreover, the exclusion of tide gauge data in the primary analysis safeguards the integrity of the study results against potential biases stemming from the absence of vertical land movement corrections.

3.2. Seasonal and Long-Term Changes of SCS Sea Level

The climatological evolution of spatially averaged model SSHA as well as the OBP and steric sea level components, over the Sunda Shelf, Northwestern Shelf and deep SCS (Figure 2c) is presented in Figures 2d–2f, respectively. The seasonal variability of sea level exhibits larger amplitudes over the shelves, with negative maxima occurring during June-July, and positive maxima in December-January. The seasonal variability of sea level over the SCS shelves is largely influenced by the mass gain or loss (Figures 2d and 2e). The steric sea level in the Sunda Shelf region exhibits an opposite phase evolution compared to the SSHA and OBP, largely following the seasonal march of the sun. The dominance of wind forcing in shaping the sea level seasonal changes over the SCS shelves is reported in earlier studies (Amiruddin et al., 2015; Cheng & Qi, 2010; Qu et al., 2019). The seasonal variability of sea level in the deep SCS is relatively weaker compared to the shelf regions, with the primary driving factor being the steric sea level (Figure 2f).

The spatial patterns of linear trends in OBP and steric sea level for the period 1961–2022 are depicted in Figures 3a and 3b, respectively. The OBP and steric sea level exhibit contrasting trends in the SCS, particularly over the deep SCS. The steric sea level exhibits a significant increasing trend of more than 5 mm yr^{-1} in the deep SCS, while its trend over the shelves is not as pronounced. Conversely, to compensate for the increase in steric sea level, the OBP demonstrates a decreasing trend, exceeding -3 mm yr^{-1} in the deep SCS. The Sunda shelf and northwestern shelf regions are characterized by an increasing OBP trend of 2–3 mm yr^{-1} during the period.

Figures 3c and 3d show the linear regression analyses of OBP and steric sea level against the model total SSHA. Over the shelf region, the OBP accounts for over 80% of the total sea level change, while the steric contribution
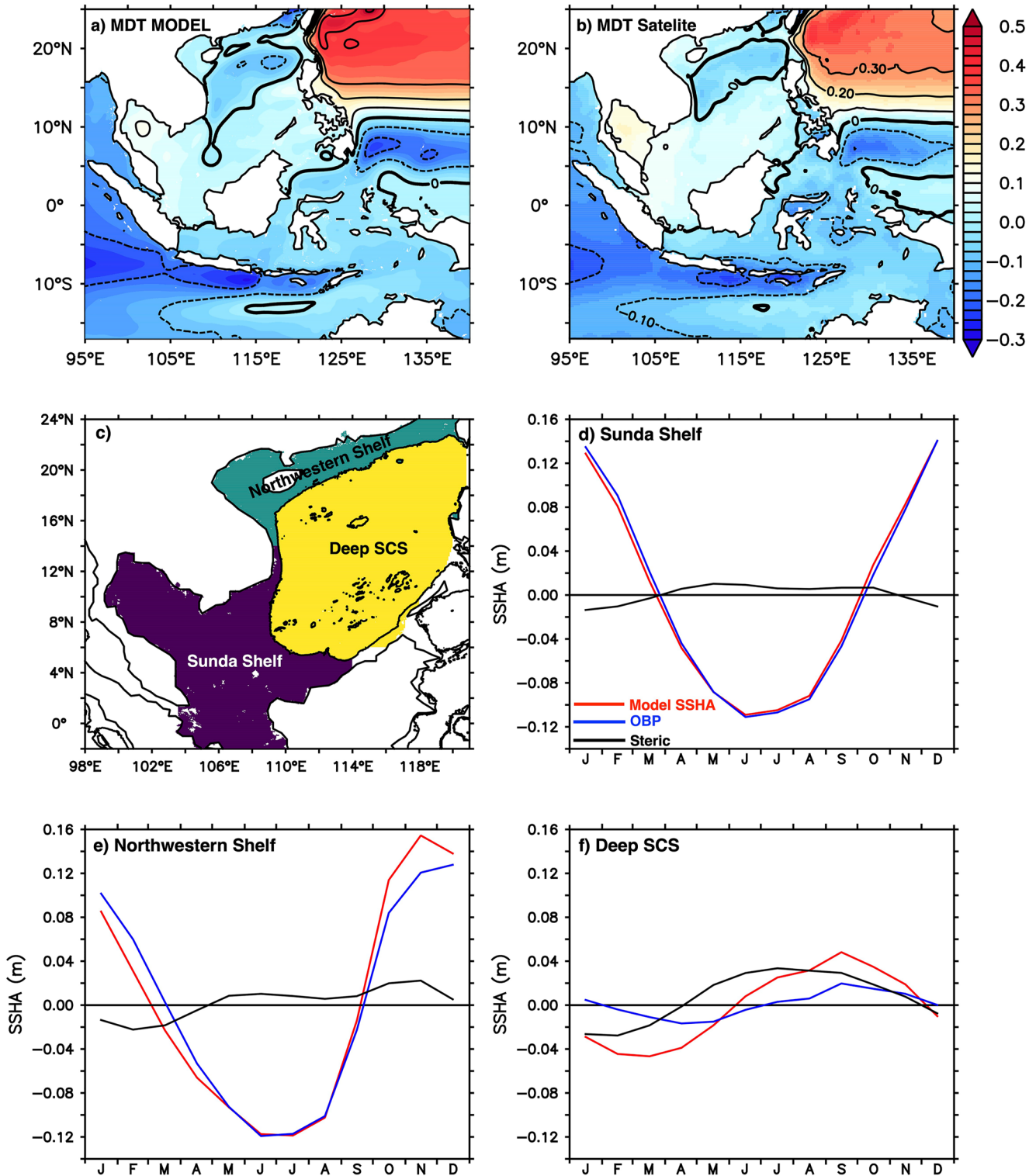
Figure 2. Comparison of (a) model-simulated and (b) satellite observed Mean Dynamic Topography (MDT) anomaly (in m) for 1993–2022. The spatial mean is removed from both, model and satellite MDT, whereas the inverse barometer effect is removed from the model. Partitioning of the study domain to the Sunda Shelf, Northwestern Shelf and Deep South China Sea (SCS) regions is depicted in (c). The spatial average of climatological model sea surface height anomaly (SSHA), ocean bottom pressure and steric sea level are shown for (d) Sunda Shelf, (e) Northwestern Shelf and (f) Deep SCS region. The black straight line in panels (d–f) indicates the zero SSHA.
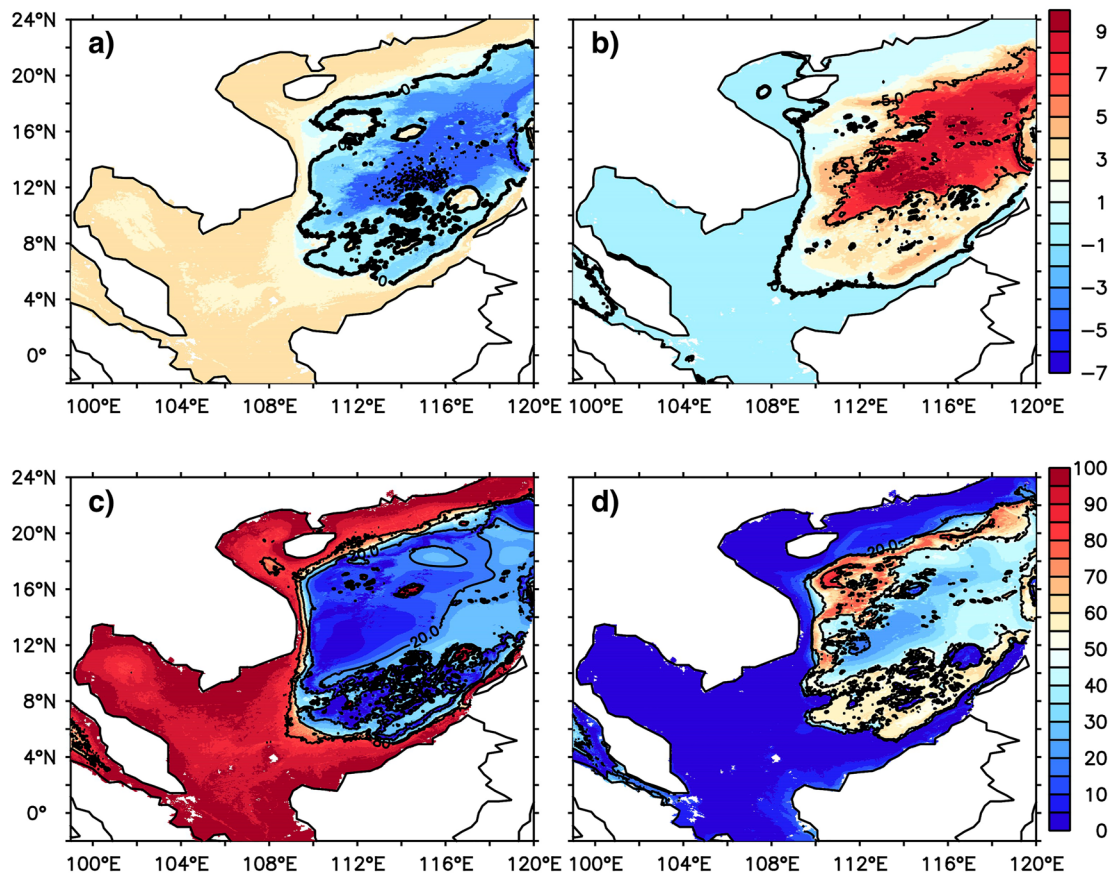
Figure 3. The linear trend (mm yr^{-1}) of the model ocean bottom pressure (OBP) (a) and steric (b) sea level components for the period 1961–2022. The relative contributions of model OBP (c) and steric sea level (d) to the model sea surface height anomaly. A 13-month low-pass filter is applied to remove the seasonal cycle from the data.

is considerably lower. On the other hand, the steric sea level is responsible for the sea level changes in the deep SCS region, contributing more than 50% to the total sea level change. Consistent findings have been reported in previous studies examining the sea level variability within the SCS (Chen et al., 2021; Jin et al., 2021).

The areal averages of the model SSHA, OBP and steric sea level during 1961–2022 over the Sunda Shelf, northwestern shelf, and deep SCS are illustrated in Figure 4. A positive sea level trend is observed over entire SCS, characterized by diverse contributions from OBP and steric components. The linear trends of model sea level over the Sunda Shelf, northwestern shelf and deep SCS during the period are 1.60 ± 0.13, 1.71 ± 0.15, and 1.47 ± 0.14 mm yr^{-1}, respectively (the uncertainty refers to error with 95% confidence interval). Consistent with our previous analysis, the OBP is attributed to more than 80% of the sea level change over the SCS shelf regions, while the contribution of steric sea level to the total sea level change is found to be less than 10%. In the deep SCS, the steric sea level and OBP display divergent characteristics compared to the shelf region. The steric sea level has exhibited a sharp increase of approximately 0.28 m during the last six decades. On the contrary, there has been a compensatory drop of around 0.18 m in ocean OBP, resulting in a net sea level change of 0.1 m over the region. The steric expansion of sea water generates a sharp pressure gradient extending from the deep SCS to the adjacent shelf regions. As a compensatory mechanism, the rapid propagation of barotropic gravity waves serves to redistribute steric sea level anomalies toward the surrounding shelf regions (Landerer et al., 2007). Eventually, this signifies a net transfer of mass onto the shelves originating from the deep SCS.

3.3. Role of Ocean Volume Transport in the SCS Regional Sea Level Changes

The transport of water between the SCS and its adjacent oceans or seas through various straits is commonly referred to as the SCS Throughflow (SCSTF) (e.g., Fang et al., 2009). Figure 1 describes the major pathways of
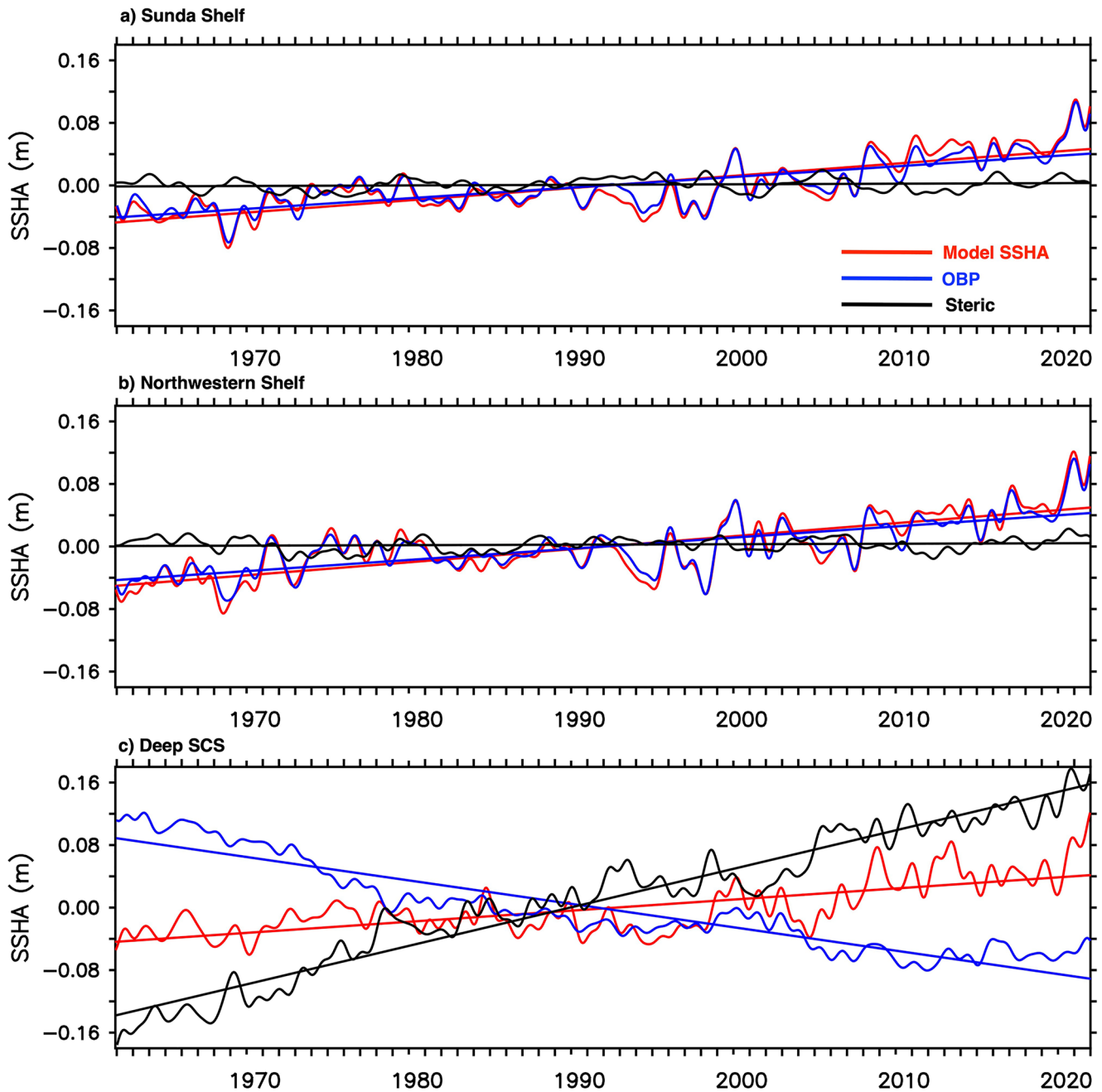
Figure 4. The spatial average of model sea surface height anomaly, ocean bottom pressure and steric sea level over the (a) Sunda Shelf, (b) Northwestern Shelf and (c) Deep South China Sea region.

inward or outward ocean water mass transport in the SCS. On an annual average basis, water from the west Pacific Ocean enters the SCS through the Luzon Strait. It then exits through various routes, including the Taiwan Strait, Mindoro-Balabac Strait, Malacca Strait, and Karimata Strait, toward the West Pacific Ocean, Sulu Sea, Andaman Sea, and Java Sea, respectively. The volume transports across various straits estimated using the model simulated current velocities are plotted in Figure 5a.

The major component of the SCSTF is the Luzon Strait transport (LST), which exhibits a net westward flow from the west Pacific Ocean to the SCS. Meanwhile, there is a net northward (outward) flow from the SCS to the East China Sea through the Taiwan Strait. The Mindoro and Balabac Straits show strong interannual variation in volume transport, with a net flow inward or outward of the SCS. The flow variability through the Mindoro and
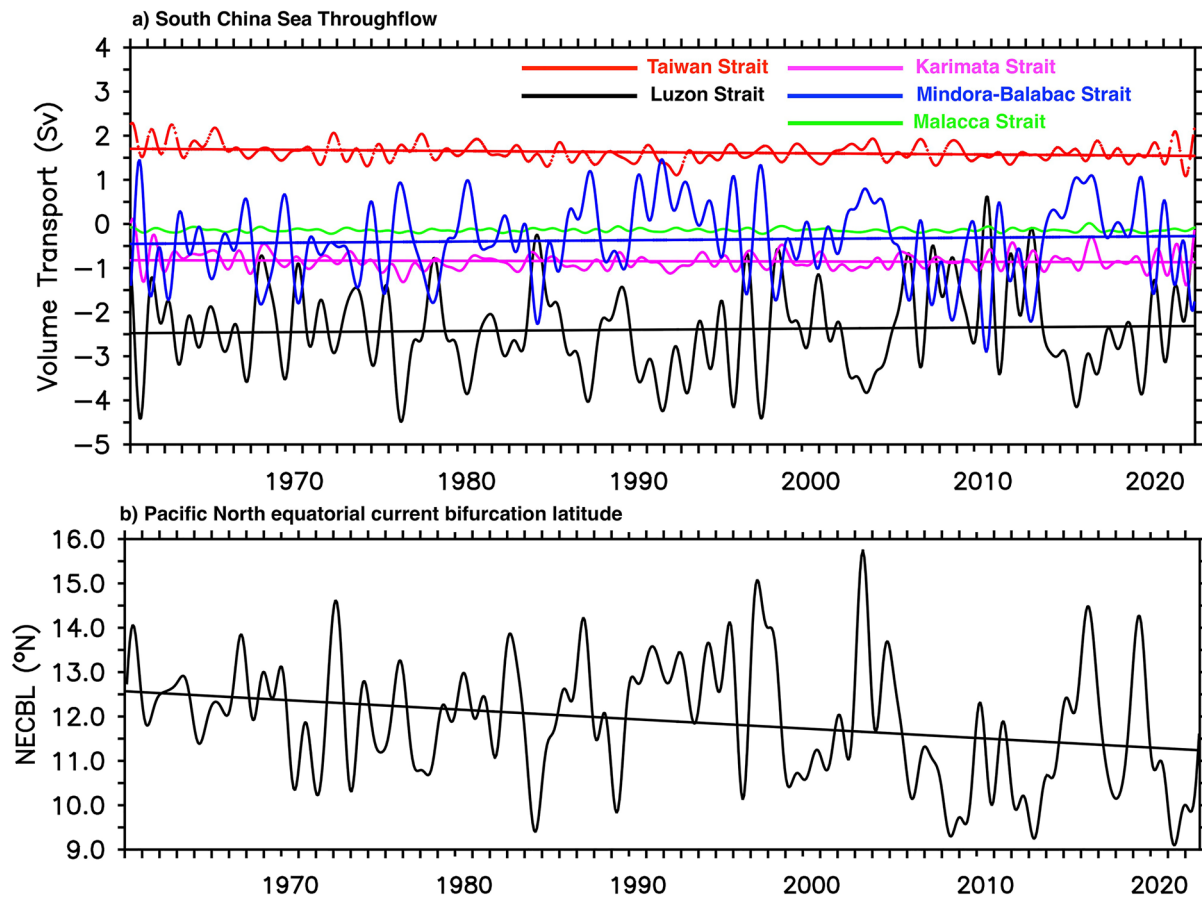
Figure 5. The components of SCSTF along with their linear trends in Sv (a) and the north equatorial current bifurcation latitude estimated from model sea surface height anomaly using equation two from Qiu and Chen (2010) (b). The seasonal cycle is removed from the time series by applying a 13-month low-pass filter. Positive values indicate northward or eastward transport, while negative values denote transport in a southward or westward direction.

Balabac Strait appears to be strongly correlated with the interannual variability of the LST. The volume transport through the Malacca and Karimata Straits shows a net outward flow from the SCS. The LST exhibits a linear decreasing trend of 0.026 ± 0.003 Sv decade^{-1} over the last six decades, indicating a weakening of flow from the Pacific Ocean to the SCS. The LST represents the portion of water intruding the SCS from the Kuroshio Current as it proceeds northward after traversing Luzon Island. Previous studies have revealed that a weakened Kuroshio Current results in an increase in the LST, while a stronger Kuroshio Current leads to a decrease in the LST (e.g., Yaremchuk & Qu, 2004). The migration of the Pacific north equatorial current bifurcation latitude (NECBL) toward the south or north has a significant impact on the strength of the Kuroshio Current (Metzger & Hurlburt, 2001). The NECBL exhibits a significant southward migration with a rate of $0.22 \pm 0.004°$ decade^{-1} during the analysis period (Figure 5b), indicating a stronger Kuroshio Current and consequently a weakening of the LST or SCSTF over this period.

Following the reduction in LST, the flow across the Taiwan and Mindoro-Balabac Straits also displays decreasing trends of 0.026 ± 0.001 and 0.028 ± 0.003 Sv decade^{-1}, respectively. Strikingly, the transport through the Karimata Strait shows a linear increasing trend of 0.007 ± 0.001 Sv decade^{-1} during the same period. This indicates an increase in ocean volume due to the processes within the SCS, likely attributed to the steric expansion in deep SCS and subsequent mass redistribution. The SCSTF acts as a cooling mechanism in the SCS, as the water flowing out through the Mindoro-Balabac and Karimata Straits is considerably warmer compared to the water entering through the Luzon Strait (e.g., Fang et al., 2009; Qu et al., 2009; Xu et al., 2023). Our analysis reveals a weakening of the SCSTF over the last six decades. The weakened SCSTF is associated with reduced heat loss from the SCS (e.g., Xiao et al., 2020), leading to enhanced heat accumulation and subsequent larger steric expansion in the deep SCS. As previously discussed, the steric expansion results in a horizontal pressure gradient, which subsequently triggers barotropic adjustment and drives the movement of water toward the shelves.

4. Conclusions

The SCS is characterized by extensive continental shelves, encompassing over 52% of the total surface area. Due to the shallow ocean depths, the steric processes are not adequate to explain the sea level changes over the shelves. The study investigated long-term sea level changes in the SCS using a validated high-resolution regional ocean model simulation. The contributions of steric sea level and OBP, which represents ocean mass redistribution, are accounted for to understand the processes associated with the sea level variations. The analysis of linear trends in OBP and steric sea level over the period 1961–2022 reveals a significant increasing trend in steric sea level of more than 5 mm yr^{-1} in the deep SCS, while the OBP exhibits a compensatory decreasing trend exceeding -3 mm yr^{-1}. The Sunda shelf and northwestern shelf regions show an increasing OBP trend during the period. The OBP accounts for over 80% of the total sea level change, with the steric contribution being relatively small over the shelf regions. Conversely, in the deep SCS region, the steric sea level emerges as the dominant factor, contributing more than 50% to the total sea level change. The steric expansion of sea water produces a sharp pressure gradient from the deep SCS to the adjacent shelves, and as a compensatory mechanism, barotropic gravity waves swiftly redistribute steric sea level anomalies to the surrounding shelf regions (e.g., Landerer et al., 2007).

The LST, considered as a representation of SCSTF, exhibits a linear decreasing trend over the last six decades, indicating a weakening flow from the Pacific Ocean to the SCS. This result is consistent with the recent studies by Zhu, Yao, Li, et al. (2022) and Zhu, Yao, Xu, et al. (2022). The southward migration of the Pacific NECBL during the analysis period is consistent with the finding of a weakening of the LST. The weakened LST results in higher heat accumulation and subsequent larger steric expansion in the deep SCS. The study revealed an increase in steric sea level within the deep SCS, leading to water redistribution toward the shelves. It is important to note that the impact of changes in land ice and groundwater storage on ocean mass redistribution, along with the uncertainties in the atmospheric and ocean reanalysis data used for model forcing, have not been addressed in this study. Further research is needed to assess the role of these factors.

Data Availability Statement

The NEMO v4.0.6 model code and documentation are freely available (NEMO v4.0.6, Madec et al., 2016). Processed model output used in the analysis is are publicly available from Zenodo (Thompson et al., 2023). The ERA5 and ORAS5 data are obtained from the Hersbach et al. (2023) and Copernicus Climate Change Service, Climate Data Store (2021), respectively. The satellite SSH data is available from (E.U. Copernicus Marine Service Information, n.d.).

References

Amiruddin, A. M., Haigh, I. D., Tsimplis, M. N., Calafat, F. M., & Dangendorf, S. (2015). The seasonal cycle and variability of sea level in the South China Sea. *Journal of Geophysical Research: Oceans*, *120*(8), 5490–5513. https://doi.org/10.1002/2015JC010923

Chen, C., Wang, G., Yan, Y., & Luo, F. (2021). Projected sea level rise on the continental shelves of the China Seas and the dominance of mass contribution. *Environmental Research Letters*, *16*(6), 064040. https://doi.org/10.1088/1748-9326/abfdea

Cheng, X., & Qi, Y. (2010). On steric and mass-induced contributions to the annual sea-level variations in the South China Sea. *Global and Planetary Change*, *72*(3), 227–233. https://doi.org/10.1016/j.gloplacha.2010.05.002

Copernicus Climate Change Service, Climate Data Store. (2021). ORAS5 global ocean reanalysis monthly data from 1958 to present [Dataset]. Copernicus Climate Change Service (C3S) Climate Data Store (CDS). https://doi.org/10.24381/cds.67e8eeb7

E.U. Copernicus Marine Service Information. (n.d.). Global ocean gridded L 4 sea surface heights and derived variables reprocessed Copernicus Climate Service [Dataset]. E.U. Copernicus Marine Service Information (CMEMS). Marine Data Store (MDS). https://doi.org/10.48670/moi-00145

Fang, G., Yonggang, W., Zexun, W., Yue, F., Fang-Li, Q., & Xiaomin, H. (2009). Interocean circulation and heat and freshwater budgets of the South China Sea based on a numerical model. *Dynamics of Atmospheres and Oceans*, *47*(1–3), 55–72. https://doi.org/10.1016/j.dynatmoce.2008.09.003

Fox-Kemper, B., Hewitt, H. T., Xiao, C., Adalgeirsdottir, G., Drijfhout, S. S., Edwards, T. L., et al. (2021). Ocean, cryosphere and sea level change. In *Climate Change 2021: The Physical Science Basis. Contribution of Working Group I to the Sixth Assessment Report of the Intergovernmental Panel on Climate Change* (pp. 1211–1362). Cambridge University Press. https://doi.org/10.1017/9781009157896.011

GEBCO Compilation Group. (2020). GEBCO 2020 grid. https://doi.org/10.5285/a29c5465-b138-234d-e053-6c86abc040b9

Gregory, J. M., Griffies, S. M., Hughes, C. W., Lowe, J. A., Church, J. A., Fukimori, I., et al. (2019). Concepts and terminology for sea level: Mean, variability and change, both local and global. *Surveys in Geophysics*, *40*(6), 1251–1289. https://doi.org/10.1007/s10712-019-09525-z

Hersbach, H., Bell, B., Berrisford, P., Biavati, G., Horányi, A., Muñoz Sabater, J., et al. (2023). ERA5 hourly data on single levels from 1940 to present [Dataset]. Copernicus Climate Change Service (C3S) Climate Data Store (CDS). https://doi.org/10.24381/cds.adbb2d47

Hersbach, H., Bell, B., Berrisford, P., Hirahara, S., Horányi, A., Muñoz-Sabater, J., et al. (2020). The ERA5 global reanalysis. *Quarterly Journal of Royal Meteorology Society*, *146*(730), 1999–2049. https://doi.org/10.1002/qj.3803

Holgate, S. J., Matthews, A., Woodworth, P. L., Rickards, L. J., & Tamisiea, M. E. (2013). New data systems and products at the permanent service for mean sea level. *Journal of Coastal Research*, *29*(3), 493–504. https://doi.org/10.2112/JCOASTRES-D-12-00175.1

IPCC. (2023). Summary for policymakers. In Core Writing Team, H. Lee, & J. Romero (Eds.), *Climate Change 2023: Synthesis Report. A Report of the Intergovernmental Panel on Climate Change. Contribution of Working Groups I, II and III to the Sixth Assessment Report of the Intergovernmental Panel on Climate Change* (p. 36). IPCC. (in press).

Jin, Y., Zhang, X., Church, J. A., & Bao, X. (2021). Projected sea level changes in the marginal seas near China based on dynamical downscaling. *Journal of Climate*, *34*, 7037–7055. https://doi.org/10.1175/JCLI-D-20-0796.1

Landerer, F. W., Jungclaus, J. H., & Marotzke, J. (2007). Ocean bottom pressure changes lead to a decreasing length-of-day in a warming climate. *Geophysical Research Letters*, *34*(6), L06307. https://doi.org/10.1029/2006GL029106

Madec, G., & the NEMO team. (2016). *NEMO reference manual 3_6_STABLE: NEMO ocean engine. Note du Pôle de modélisation* (Vol. 27). Institut Pierre-Simon Laplace (IPSL).

Metzger, E. J., & Hurlburt, H. E. (2001). The nondeterministic nature of Kuroshio penetration and eddy shedding in the South China Sea. *Journal of Physical Oceanography*, *31*(7), 1713–1732. https://doi.org/10.1175/1520-0485(2001)031<1712:TNNOKP>2.0.CO;2

Mitrovica, J. X., Tamisiea, M. E., Davis, J. L., & Milne, G. A. (2001). Recent mass balance of polar ice sheets inferred from patterns of global sea-level change. *Nature*, *409*(6823), 1026–1029. https://doi.org/10.1038/35059054

Peltier, W. R. (2004). Global glacial isostasy and the surface of the ice-age Earth: The ICE-5G (VM2) model and GRACE. *Annual Review of Earth and Planetary Sciences*, *32*(1), 111–149. https://doi.org/10.1146/annurev.earth.32.082503.144359

Qiu, B., & Chen, S. (2010). Interannual-to-decadal variability in the bifurcation of the north equatorial current off the Philippines. *Journal of Physical Oceanography*, *40*(11), 2525–2538. https://doi.org/10.1175/2010JPO4462.1

Qu, T., Song, T., & Yamagata, T. (2009). An introduction to the South China Sea throughflow: Its dynamics, variability, and application for climate. *Dynamics of Atmospheres and Oceans*, *47*(1–3), 3–14. https://doi.org/10.1016/j.dynatmoce.2008.05.001

Qu, Y., Jevrejeva, S., Jackson, L. P., & Moore, J. C. (2019). Coastal Sea level rise around the China Seas. *Global and Planetary Change*, *172*, 454–463. https://doi.org/10.1016/j.gloplacha.2018.11.005

Thompson, B., Jevrejeva, S., Zachariah, J., Faller, G. D., & Tkalich, P. (2023). Modelled sea surface height and components in the South China Sea [Dataset]. Zenodo. https://doi.org/10.5281/zenodo.8201618

Wunsch, C., & Stammer, D. (1997). Atmospheric loading and the oceanic "inverted barometer" effect. *Reviews of Geophysics*, *35*(1), 79–107. https://doi.org/10.1029/96RG03037

Xiao, F., Wang, D., & Yang, L. (2020). Can tropical Pacific winds enhance the footprint of the Interdecadal Pacific Oscillation on the upper-ocean heat content in the South China Sea? *Journal Climate*, *33*(10), 4419–4437. https://doi.org/10.1175/JCLI-D-19-0679.1

Xu, Q., Zhang, L., Xiao, X., Zhou, C., Wang, F., & Hu, D. (2023). Seasonal link between deepwater overflow through the Luzon Strait and deep western boundary current in the Philippine Sea. *Geophysical Research Letters*, *50*(18), e2023GL105405. https://doi.org/10.1029/2023GL105405

Yaremchuk, M., & Qu, T. (2004). Seasonal variability of the large-scale currents near the coast of the Philippines. *Journal of Physical Oceanography*, *34*(4), 844–855. https://doi.org/10.1175/1520-0485(2004)034<0844:SVOTLC>2.0.CO;2

Zhu, Y., Yao, J., Li, S., Xu, T., Huang, R. X., Nie, X., et al. (2022). Decadal weakening of abyssal South China Sea circulation. *Geophysical Research Letters*, *49*(20), e2022GL100582. https://doi.org/10.1029/2022GL100582

Zhu, Y., Yao, J., Xu, T., Li, S., Wang, Y., & Wei, Z. (2022). Weakening trend of Luzon Strait overflow transport in the past two decades. *Geophysical Research Letters*, *49*(7), e2021GL097395. https://doi.org/10.1029/2021GL097395

Zuo, H., Balmaseda, M. A., Tietsche, S., Mogensen, K., & Mayer, M. (2019). The ECMWF operational ensemble reanalysis–analysis system for ocean and sea ice: A description of the system and assessment. *Ocean Sciences*, *15*(3), 779–808. https://doi.org/10.5194/os-15-779-2019

References From the Supporting Information

Canuto, V., Howard, A., Cheng, Y., & Dubovikov, M. (2001). Ocean turbulence, Part I: One-point closure model-momentum and heat vertical diffusivities. *Journal of Physical Oceanography*, *31*(6), 1413–1426. https://doi.org/10.1175/1520-0485(2001)031<1413:OTPIOP>2.0.CO;2

Davies, H. (1976). A lateral boundary formulation for multi-level prediction models. *Quarterly Journal of Royal Meteorology Society*, *102*(432), 405–418. https://doi.org/10.1002/qj.49710243210

Edson, J. B., Jampana, V., Weller, R. A., Bigorre, S. P., Plueddemann, A. J., Fairall, C. W., et al. (2013). On the exchange of momentum over the open ocean. *Journal of Physical Oceanography*, *43*(8), 1589–1610. https://doi.org/10.1175/JPO-D-12-0173.1

Flather, R. A. (1976). A tidal model of the northwest European continental shelf. *Mémoires de la Société royale des sciences de Liège*, *10*, 141–164.

Lengaigne, M., Menkes, C., Aumont, O., Gorgues, T., Bopp, L., Madec, J., & Madec, G. (2007). Bio-physical feedbacks on the tropical Pacific climate in a coupled general circulation model. *Climate Dynamics*, *28*(5), 503–516. https://doi.org/10.1007/s00382-006-0200-2

Levier, B., Tréguier, A. M., Madec, G., & Garnier, V. (2007). Free surface and variable volume in the NEMO code (Technical report). *MERSEA MERSEA IP Report WP09-CNRS-STR-03-1A* (p. 47). https://doi.org/10.5281/zenodo.3244182

Umlauf, L., & Burchard, H. (2013). A generic length-scale equation for geophysical turbulence models. *Journal of Marine Research*, *61*(2), 235–265. https://doi.org/10.1357/002224003322005087